STRUCTURAL BIOLOGY COMMUNICATIONS

ISSN 2053-230X

The structure of the metallo-β-lactamase VIM-2 in complex with a triazolylthioacetamide inhibitor

Tony Christopeit,[a] Ke-Wu Yang,[b] Shao-Kang Yang[b] and Hanna-Kirsti S. Leiros[a]*

[a]The Norwegian Structural Biology Centre (Norstruct), Department of Chemistry, Faculty of Science and Technology, UiT The Arctic University of Norway, N-9037 Tromsø, Norway, and [b]Key Laboratory of Synthetic and Natural Functional Molecule Chemistry of Ministry of Education, College of Chemistry and Materials Science, Northwest University, Xi'an 710127, People's Republic of China. *Correspondence e-mail: hanna-kirsti.leiros@uit.no

Received 26 August 2016
Accepted 11 October 2016

Edited by W. N. Hunter, University of Dundee, Scotland

Keywords: antibiotic resistance; DMSO-free co-crystallization; carbapenemases; VIM-2; metallo-β-lactamases.

PDB reference: VIM-2 in complex with a triazolylthioacetamide inhibitor, 5lsc

Supporting information: this article has supporting information at journals.iucr.org/f

The increasing number of pathogens expressing metallo-β-lactamases (MBLs), and in this way achieving resistance to β-lactam antibiotics, is a significant threat to global public health. A promising strategy to treat such resistant pathogens is the co-administration of MBL inhibitors together with β-lactam antibiotics. However, an MBL inhibitor suitable for clinical use has not yet been identified. Verona integron-encoded metallo-β-lactamase 2 (VIM-2) is a widespread MBL with a broad substrate spectrum and hence is an interesting drug target for the treatment of β-lactam-resistant infections. In this study, three triazolylthioacetamides were tested as inhibitors of VIM-2. One of the tested compounds showed clear inhibition of VIM-2, with an IC_{50} of 20 μ*M*. The crystal structure of the inhibitor in complex with VIM-2 was obtained by DMSO-free co-crystallization and was solved at a resolution of 1.50 Å. To our knowledge, this is the first structure of a triazolylthioacetamide inhibitor in complex with an MBL. Analysis of the structure shows that the inhibitor binds to the two zinc ions in the active site of VIM-2 and revealed detailed information on the interactions involved. Furthermore, the crystal structure showed that binding of the inhibitor induced a conformational change of the conserved residue Trp87.

1. Introduction

The discovery of β-lactam antibiotics for the treatment of bacterial infections has revolutionized modern medicine and saved countless lives. Unfortunately, the overuse of these antibiotics has resulted in the rapid emergence of β-lactam-resistant bacteria, representing a major threat to global public health (World Health Organization, 2014). A main mechanism for bacteria to develop resistance to β-lactam antibiotics is the expression of β-lactamases, enzymes that are able to hydrolyse the β-lactam ring and render the antibiotics ineffective. The co-administration of β-lactamase inhibitors together with β-lactam antibiotics can prevent their hydrolysis and in this way overcome resistance. To date, two different groups of β-lactamases have been identified: metallo-β-lactamases (MBLs) and serine β-lactamases (SBLs). For SBLs, potent inhibitors co-administered with β-lactam antibiotics are already in clinical use (Drawz & Bonomo, 2010; Lucasti *et al.*, 2016). However, no MBL inhibitors have yet reached clinical use, and hence there is a clear need to identify novel inhibitors (Fast & Sutton, 2013).

Verona integron-encoded metallo-β-lactamase 2 (VIM-2) is a widespread MBL with a broad substrate spectrum, including penicillins, cephalosporins, cephamycins and carbapenems (Poirel *et al.*, 2000). In its mature form, VIM-2 is a monomeric enzyme consisting of 240 amino acids with a molecular mass of 25 kDa (Docquier *et al.*, 2003; Garcia-Saez *et al.*, 2008).

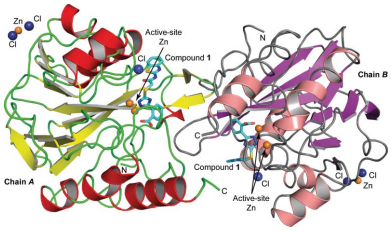

Table 1
Crystallization.

Method	Sitting-drop vapour diffusion in a new DMSO-free co-crystallization method
Plate type	MRC 96-well crystallization plate (Molecular Dimensions)
Temperature (°C)	22
Protein concentration (mg ml^{-1})	9.4
Buffer composition of protein solution	50 m*M* Tris–HCl pH 7.2, 100 µ*M* $ZnCl_2$
Composition of reservoir solution	22–27% PEG 3350, 0.2 *M* magnesium formate
Volume and ratio of drop	2 µl, 1:1
Volume of reservoir	60 µl

Several crystal structures of VIM-2 have been reported (Garcia-Saez *et al.*, 2008; Aitha *et al.*, 2014). The structures show that the enzyme is folded in an $\alpha\beta/\beta\alpha$ sandwich and that two zinc ions bridged by a hydroxide are located in the active site. Furthermore, crystal structures of different inhibitors in complex with VIM-2 have been reported (Brem *et al.*, 2014, 2016; Christopeit *et al.*, 2015). VIM-2 has a high clinical relevance owing to its wide spread and broad substrate range, and therefore reflects an important drug target for the treatment of antibiotic-resistant infections.

Triazolylthioacetamides have been identified as inhibitors of different MBLs and hence are interesting scaffolds for the design of potent VIM-2 inhibitors (Zhang *et al.*, 2014; Yang *et al.*, 2015; Zhai *et al.*, 2016). In this study, we tested three different substituted triazolylthioacetamides as inhibitors of VIM-2. Moreover, the complex structure of one of the inhibitors bound to VIM-2 is presented and protein–inhibitor interactions are explored.

2. Materials and methods

2.1. Expression and purification of VIM-2

The expression and purification of VIM-2 was carried out as described previously (Christopeit *et al.*, 2015). In brief, the gene sequence coding for residues Val25–Glu300 of VIM-2 was isolated from *Pseudomonas aeruginosa* strain 301-5473. The sequence for a 6×His tag and a *Tobacco etch virus* (TEV) protease cleavage site was added and the construct was transferred into pDEST14 vector. Chemically competent *Escherichia coli* BL21(DE3)pLysS cells (Invitrogen) were transformed with the VIM-2 pDEST14 vector and cultured at 37°C in Terrific broth (TB) medium supplemented with 100 mg l^{-1} ampicillin and 34 mg l^{-1} chloramphenicol. Protein expression was induced overnight at 20°C with 0.4 m*M* isopropyl β-D-1-thiogalactopyranoside (IPTG). The cells were harvested by centrifugation and stored at −80°C. Sonication was used to lyse the cells and insoluble material was removed by centrifugation. The supernatant was applied onto a HisTrap HP column (GE Healthcare) and bound VIM-2 was eluted with a linear imidazole gradient. The His tag was removed by adding in-house-produced His-tagged TEV protease. The cleaved His tag, uncleaved protein and the His-tagged TEV protease were removed by performing a second HisTrap purification. The flowthrough containing VIM-2 was collected and the protein was finally purified by anion-exchange chromatography. The purity of the enzyme was analysed by SDS–PAGE and the activity was confirmed by the hydrolysis of nitrocefin. The protein concentration was determined by measuring the absorption at 280 nm using a NanoDrop 2000c spectrophotometer (Thermo Scientific). The extinction coefficient of 29 910 M^{-1} cm^{-1} at 280 nm was estimated from the amino-acid sequence of VIM-2 using *ProtParam* (Gasteiger *et al.*, 2005).

2.2. Synthesis of compounds 1, 2 and 3

Compound **1** was synthesized and characterized as described previously by Yang *et al.* (2015) and compounds **2** and **3** as described previously by Zhang *et al.* (2014). All compounds were dissolved in DMSO at a concentration of 100 m*M* and stored at ∼20°C.

2.3. Enzyme-inhibition assay and IC_{50} determination

The IC_{50} values were determined using a previously established enzyme-activity assay based on the hydrolysis of nitrocefin (Christopeit *et al.*, 2015). Measurements were carried out at 25°C in 96-well plates using a SpectraMax M2e (Molecular Devices). Data were analysed using the *SoftMax Pro* 5.2 software (Molecular Devices) and *GraphPad Prism* 5 (GraphPad Software). A buffer consisting of 50 m*M* HEPES pH 7.2, 150 m*M* NaCl, 100 µ*M* $ZnCl_2$, 0.005% Tween 20, 2.5% DMSO and 20 µg ml^{-1} bovine serum albumin (BSA) was used in all measurements. The inhibitors were dissolved in buffer in a twofold dilution series and mixed with VIM-2. After 5 min of incubation, the enzyme reaction was started by adding nitrocefin (Calbiochem) to a final concentration of 3 µ*M*. The final enzyme concentration was 150 p*M*. The hydrolysis of nitrocefin was followed by measurement of the absorption at 482 nm every 17 s for 20 min. The initial velocity was determined and the percentage of inhibition was calculated in relation to a positive control without inhibitor. The percentage of inhibition was plotted against the inhibitor concentration and the data were fitted to a dose–response curve with a constant top plateau (100%), a constant bottom plateau (0%) and a constant Hill slope of −1.

2.4. Crystallization, X-ray data collection and structure determination

VIM-2 was crystallized by the sitting-drop vapour-diffusion method (Table 1) using a new DMSO-free co-crystallization method. The reservoir wells of an MRC 96-well crystallization plate (Molecular Dimensions) were pre-coated with the inhibitor. 3 µl of compound **1** (100 m*M*) dissolved in DMSO was added to every reservoir well and the DMSO was evaporated by leaving the plate open in a fume hood for 24 h. After evaporation of the DMSO, 60 µl of reservoir solution was added consisting of 22–27% polyethylene glycol (PEG) 3350, 0.2 *M* magnesium formate. The 96-well plate was placed on a shaker for 24 h to dissolve the inhibitor in the reservoir solution. The reservoir solution was mixed with the protein solution (9.4 mg ml^{-1}) in a 1:1 ratio and crystals appeared

Table 2
Data collection.

Values in parentheses are for the outer shell.

Diffraction source	MX beamline BL14.1, BESSY II
Wavelength (Å)	0.918409
Temperature (°C)	−173
Detector	PILATUS 6M
Crystal-to-detector distance (mm)	297
Rotation range per image (°)	0.1
Total rotation range (°)	200
Exposure time per image (s)	0.4
Space group	*C*2
a, *b*, *c* (Å)	100.62, 79.25, 67.20
α, *β*, *γ* (°)	90.0, 90.0, 130.5
Resolution range (Å)	38.25–1.50 (1.52–1.50)
No. of unique reflections	63893
Multiplicity	3.7 (3.6)
Completeness (%)	99.1 (93.3)
R_{merge} (%)	4.8 (30.9)
Mean $\langle I/\sigma(I)\rangle$	18.8 (4.3)
Overall *B* factor from Wilson plot (Å^2)	12.12

Table 3
Refinement statistics.

PDB code	5lsc
Final R_{work} (%)	13.55
Final R_{free} (%)	16.55
No. of non-H atoms	
Protein	3901 (chains *A* and *B*)
Ions	6 Zn^{2+}, 6 Cl^-
Compound **1**	56 (2 molecules)
Water	644
R.m.s. deviations	
Bonds (Å)	0.008
Angles (°)	1.233
Average *B* factors (Å^2)	
Protein	17.6
Ion	15.9
Compound **1** (occupancy)	21.3 (0.99/0.98)
Water	32.1
Ramachandran plot	
Most favoured (%)	98.3
Allowed (%)	1.5

after 2–14 d. For cryoprotection, crystals were transferred to 25% PEG 3350, 0.2 *M* $MgCl_2$, 15% ethylene glycol, 50 m*M* HEPES pH 7.2 and were flash-cooled in liquid nitrogen. X-ray data were collected on beamline BL14.1 operated by the Joint Berlin MX-Laboratory at the BESSY II electron-storage ring (Mueller *et al.*, 2012). Statistics for data collection are shown in Table 2. *XDS*, *POINTLESS* and *AIMLESS* were used to integrate, scale and truncate the data set and to determine the space group (Kabsch, 2010; Evans, 2006, 2011; Evans & Murshudov, 2013). The phase problem was solved by molecular replacement using *Phaser* (McCoy *et al.*, 2007) and a previously published VIM-2 structure (PDB entry 1ko3; Garcia-Saez *et al.*, 2008). The final structure was obtained by manual model optimization in *WinCoot* according to the $2F_o - F_c$ and $F_o - F_c$ electron-density maps and several refinement cycles using *PHENIX* (Emsley *et al.*, 2010; Adams *et al.*, 2010). Translation/libration/screw (TLS) parameters were used in the refinement process. Alternative rotamers were manually modelled in *WinCoot* and refined as implemented in *PHENIX*. Noncrystallographic symmetry (NCS) restraints were not used during the refinement. For all Zn^{2+} and Cl^- ions, anisotropic *B* factors and occupancies were refined by *PHENIX*. 5% of the X-ray data were used for R_{free} cross-validation. Refinement statistics are shown in Table 3. The *PyMOL* Molecular Graphics System v.1.4.1 (Schrödinger) and *LIGPLOT* were used to generate illustrations and to visualize interactions (Wallace *et al.*, 1995). The class B *β*-lactamase numbering system is used for the numbering of all residues (Garau *et al.*, 2004).

3. Results and discussion

3.1. Inhibition of VIM-2 by triazolylthioacetamides

In a previous study, we established a nitrocefin-based enzyme-activity assay suitable to study the influence of inhibitors on the activity of VIM-2 (Christopeit *et al.*, 2015). This

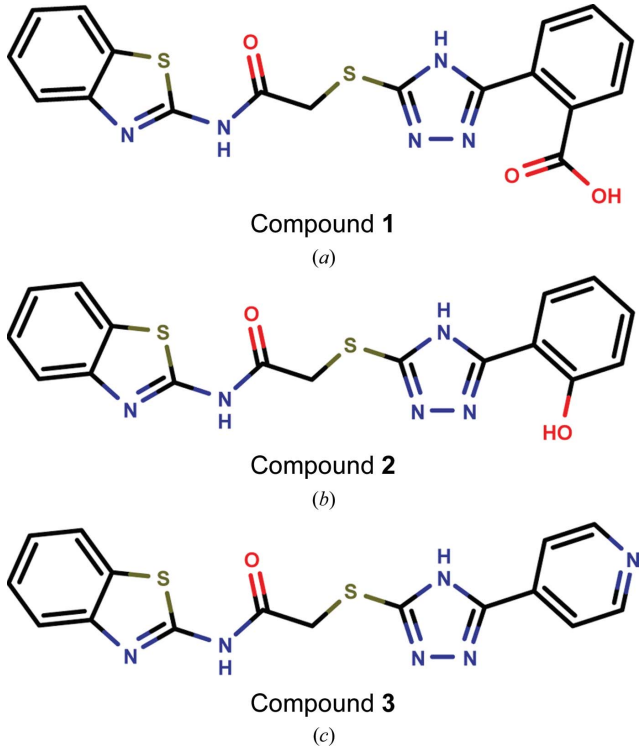

Figure 1
Structures of the tested triazolylthioacetamide inhibitors: compound **1** (*a*), compound **2** (*b*) and compound **3** (*c*).

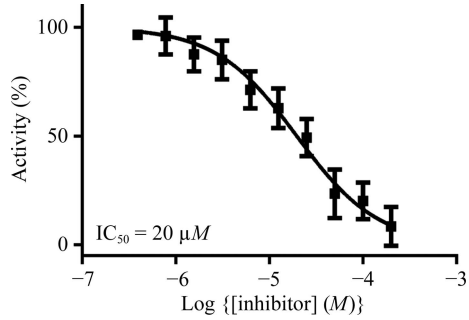

Figure 2
Dose–response curve for the inhibition of VIM-2 by compound **1**.

assay was used to determine the inhibition potency of three substituted triazolylthioacetamides (Fig. 1). All three compounds have previously been reported as inhibitors of different MBLs (Yang *et al.*, 2015; Zhang *et al.*, 2014). However, only compound **1** showed clear inhibition of VIM-2, whereas compounds **2** and **3** had no influence on the enzyme activity at concentrations of up to 100 µ*M* (data not shown). To determine the IC_{50} for compound **1**, the inhibition at different concentrations was measured and the data were fitted to a dose–response curve (Fig. 2). The IC_{50} was calculated to be 20 µ*M* (pIC_{50} = 4.71 ± 0.04).

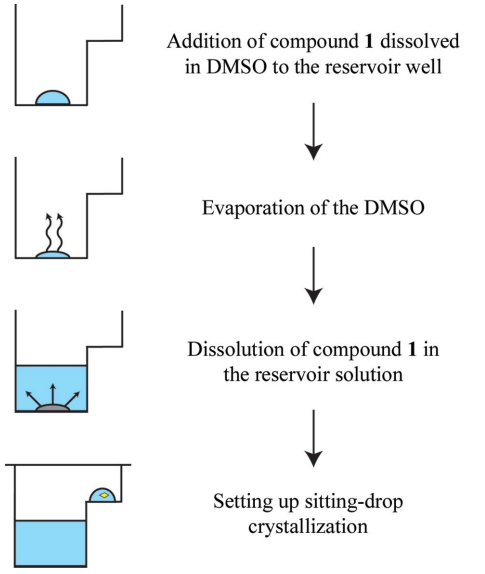

Figure 3
Strategy for DMSO-free co-crystallization of VIM-2 with compound **1**. After adding compound **1** to the reservoir well, the DMSO was evaporated and compound **1** was redissolved in the reservoir solution. The reservoir solution was mixed with the protein solution to set up sitting-drop experiments.

3.2. DMSO-free co-crystallization of VIM-2 with compound 1

We have previously reported crystal structures of VIM-2 in complex with small fragments (Christopeit *et al.*, 2015). These complex structures were obtained by solving the fragments in DMSO and soaking them into native VIM-2 crystals. However, the soaking time was limited by the negative influence of DMSO on the crystal quality and soaking was not successful for compound **1**. Furthermore, adding compound **1** directly to the reservoir or protein solution prevented crystal formation, most likely owing to the high DMSO concentration. Therefore, a DMSO-free co-crystallization strategy was explored in which the reservoir wells were pre-coated with compound **1** (Fig. 3). To achieve the pre-coating, the dissolved inhibitor was added to the reservoir wells and the DMSO was removed by evaporation. Afterwards, the inhibitor was redissolved in the reservoir solution, which was then used to set up the crystallization experiments. The structures obtained from crystals prepared by the DMSO-free co-crystallization showed additional electron density in the active site of VIM-2 corresponding to compound **1**. Although the pre-coating of sitting-drop wells with ligands has been reported before (Gelin *et al.*, 2015), to our knowledge the pre-coating of reservoir wells with ligands has not been used for co-crystallization.

3.3. Complex structure of VIM-2 with compound 1

The crystal structure of VIM-2 in complex with compound **1** was solved by molecular replacement to a resolution of 1.5 Å. The complex crystallized in space group *C*2, with two protein molecules in the asymmetric unit (Fig. 4). Details of the refinement statistics are shown in Table 3. The overall completeness of the data set was 99.1%, with a multiplicity of 3.7 and an R_{merge} of 4.8%. The overall structures of the two VIM-2 molecules in the asymmetric unit were similar, with an

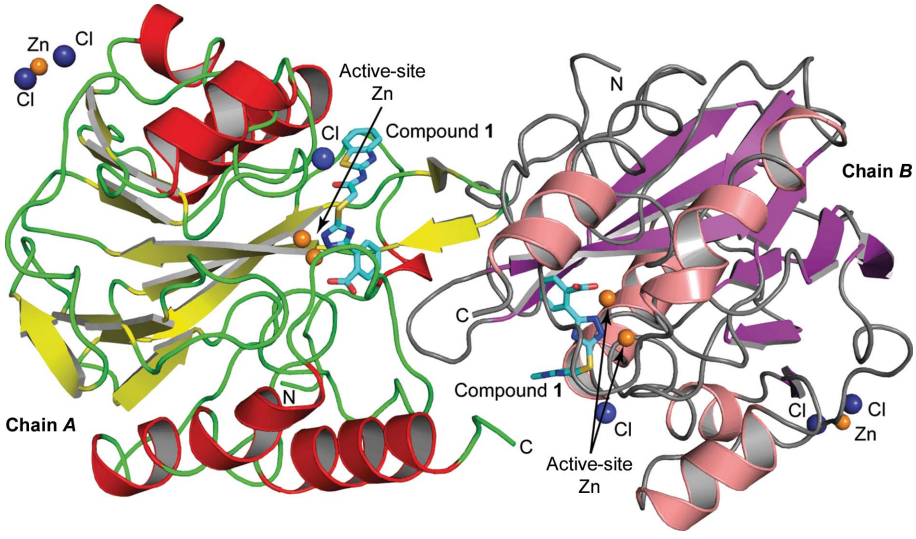

Figure 4
Ribbon diagram of the two VIM-2 molecules in the asymmetric unit. Helices are shown in red (chain *A*) or salmon (chain *B*) and β-strands are shown in yellow (chain *A*) or purple (chain *B*). The inhibitor bound to the active site is shown in stick representation with atom-type colouring and C atoms depicted in cyan. Zn^{2+} ions are shown as orange spheres and Cl^{-} ions as dark blue spheres.

r.m.s. deviation of 0.36 Å for the C^{α} atoms (*WinCoot*; Emsley *et al.*, 2010).

As is typical for MBLs, VIM-2 was folded in an $\alpha\beta/\beta\alpha$ sandwich. Two Zn^{2+} ions were observed in the active site of the enzyme, where Zn1 was coordinated by His116, His118 and His196, and Zn2 was coordinated by Asp120, Cys221 and His263. Between the two symmetry mates, a third Zn^{2+} ion was located, which has been observed before and is normally

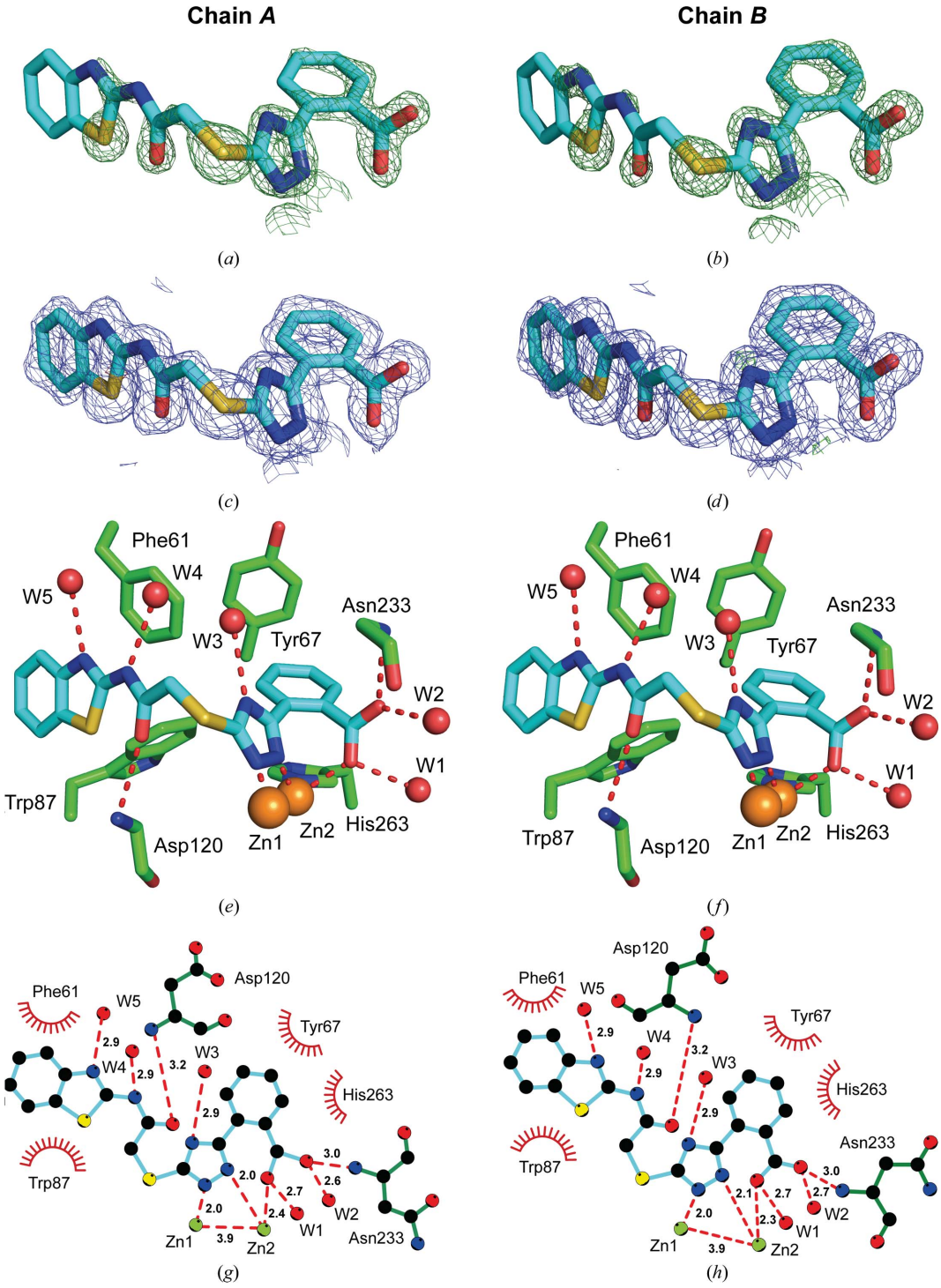

Figure 5
OMIT maps (*a*, *b*), final density maps (*c*, *d*) and crystal structures (*e*, *f*) of compound **1** bound to the active site of VIM-2. The complex crystallized with two copies in the asymmetric unit (chains *A* and *B*). C atoms of compound **1** are depicted in blue and VIM-2 C atoms in green. Water molecules are shown in red and Zn^{2+} ions in orange. The OMIT $F_o - F_c$ maps are shown in dark green at 2.25σ. The final $2F_o - F_c$ electron-density maps around the ligand are shown in blue at 1σ. The final $F_o - F_c$ difference density maps around the ligand are shown at 4σ (light green) and −4σ (red). The interactions were analysed using *LIGPLOT* (*g*, *h*). Hydrogen bonds are shown as red dashed lines and interatomic distances are given in Å. Hydrophobic interactions are indicated by red arcs.

considered to be a crystallographic artefact. The overall protein structure and the coordination of the Zn^{2+} ions, as well as the Zn–ligand and Zn–Zn distances, were in agreement with previously published VIM-2 structures (Garcia-Saez *et al.*, 2008; Aitha *et al.*, 2014; Christopeit *et al.*, 2015; Yamaguchi *et al.*, 2007).

In the active site of both VIM-2 molecules, additional electron density corresponding to a chloride ion was observed. The ions showed high occupancy, and the *B* factors of 17.3 and 20.5 Å^2 for chains *A* and *B*, respectively, were consistent with the average *B* factor of the protein (Table 3). Although the chloride ions were in proximity to the bound inhibitor, they showed no direct interaction. The ions were coordinated by the backbone N atom of Asp119, the side-chain N atom of Asn165 and one or three water molecules. To our knowledge, chloride ions at this position in the active site of VIM-2 have not been observed before. However, it is not clear whether the chloride ion has any biological relevance or whether it is a crystallographic artefact.

The experimental electron-density map clearly showed additional density corresponding to compound **1** in the active site of both VIM-2 molecules in the asymmetric unit (Fig. 5). The carboxyl group of the inhibitor interacts with Zn2 and forms hydrogen bonds to two water molecules and the backbone O atom of Asn233. Similar interactions have been observed before for fragments binding to the active site of VIM-2 (Christopeit *et al.*, 2015). The importance of this interaction for inhibitor binding is reflected by the fact that replacing the carboxyl group by a hydroxide group, as in compound **2**, or replacing the benzoic acid moiety by an 4-pyridyl moiety, as in compound **3**, resulted in a strong reduction in the inhibitory potency. The triazole ring of compound **1** interacted with both zinc ions and replaced the hydroxide molecule that normally bridges the two zinc ions in the native structure of VIM-2 (Christopeit *et al.*, 2015; Garcia-Saez *et al.*, 2008). Furthermore, the benzothiazole ring formed parallel π–π stacking with Phe61 and T-shaped π–π stacking with Trp87. Compared with our previously published structures of native VIM-2 and of VIM-2 in complex with fragments (Christopeit *et al.*, 2015), the binding of compound **1** induced a flip of the backbone and a 180° flip of the side chain of Trp87 (Fig. 6). Penicillins are well known substrates of VIM-2 and several of them have bulky hydrophobic groups, *e.g.* ampicillin or benzylpenicillin (Poirel *et al.*, 2000). The interactions involved in the binding of different substrates to VIM-2 are not exactly known and no crystal structures in complex with these substrates have been reported. However, the structure of New Delhi metallo-β-lactamase 1 (NDM-1) in complex with hydrolysed benzylpenicillin has been reported (King *et al.*, 2012). This structure shows that the bulky hydrophobic group of benzylpenicllin forms similar interactions with the conserved residue Trp87 in NDM-1 as compound **1** forms with Trp87 in VIM-2 (Fig. 7). Hence, it is likely that the binding of substrates with bulky hydrophobic groups to the active site of VIM-2 also induces the same conformational changes of Trp87 as compound **1**.

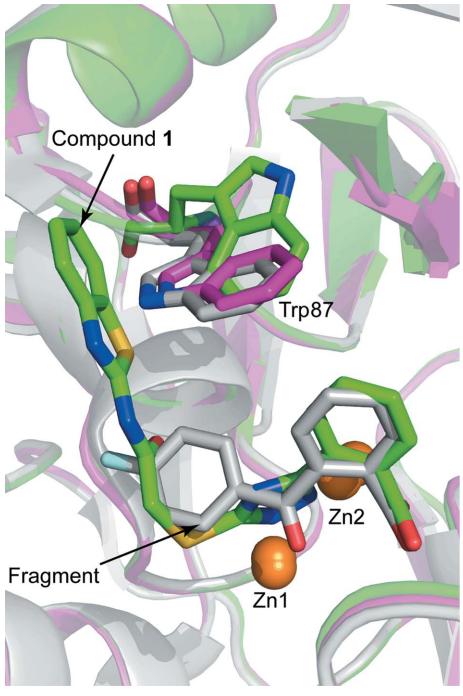

Figure 6
Structural alignment of a native VIM-2 structure (purple; PDB entry 5acu; Christopeit *et al.*, 2015), the VIM-2 structure in complex with compound **1** (green) and the VIM-2 structure in complex with a fragment (grey; PDB entry 5acx; Christopeit *et al.*, 2015). The protein backbones are shown as ribbon cartoons. Zinc ions are shown as orange spheres and Trp87, compound **1** and the fragment are shown as sticks.

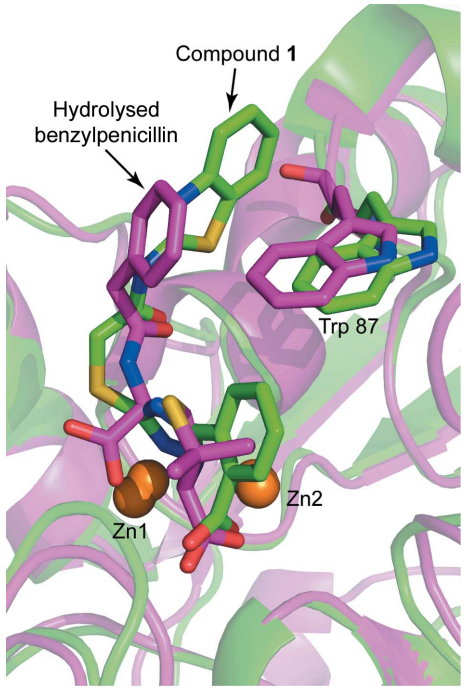

Figure 7
Structural alignment of the VIM-2 structure in complex with compound **1** (green) and a structure of NDM-1 bound to hydrolysed benzylpenicillin (purple; PDB entry 4eyf; King *et al.*, 2012). The protein backbones are shown as ribbon cartoons. Zinc ions are shown as orange spheres and Trp87, compound **1** and the fragment are shown as sticks.

4. Conclusion

In this study, compound **1** was identified as an inhibitor of the MBL VIM-2. The determined IC_{50} was in the low-micromolar range and hence needs to be further optimized. However, compound **1** has already been reported as an inhibitor of the MBLs ImiS and CcrA, and therefore is an interesting starting point for the development of broad-spectrum MBL inhibitors (Yang *et al.*, 2015). Furthermore, the crystal structure of compound **1** in complex with VIM-2 is presented. To our knowledge, this is the first structure of a triazolylthioacetamide inhibitor bound to an MBL. The detailed information about the interactions involved in the binding of the inhibitor and the induced conformational changes of the conserved residue Trp87 will help to further optimize triazolylthioacetamide inhibitors and improve rational drug design targeting MBLs.

Acknowledgements

We acknowledge Ørjan Samuelsen for supplying the *P. aeruginosa* isolate with VIM-2 and Trine Josefine O. Carlsen for the cloning and purification of VIM-2. The provision of beam time at BL14.1, BESSY II, Berlin, Germany is highly valued. This work was supported by the Tromsø Research Foundation and the Research Council of Norway (project Nos. 218539, SYNKNOYT 2011, and 213808, FRIMEDBIO 2011) and by grants 21272186, 21572179 and 81361138018 (to K-WY) from the National Natural Science Foundation of China.

References

Adams, P. D. *et al.* (2010). *Acta Cryst.* D**66**, 213–221.
Aitha, M., Marts, A. R., Bergstrom, A., Møller, A. J., Moritz, L., Turner, L., Nix, J. C., Bonomo, R. A., Page, R. C., Tierney, D. L. & Crowder, M. W. (2014). *Biochemistry*, **53**, 7321–7331.
Brem, J., van Berkel, S. S., Aik, W., Rydzik, A. M., Avison, M. B., Pettinati, I., Umland, K.-D., Kawamura, A., Spencer, J., Claridge, T. D. W., McDonough, M. A. & Schofield, C. J. (2014). *Nature Chem.* **6**, 1084–1090.
Brem, J., van Berkel, S. S., Zollman, D., Lee, S. Y., Gileadi, O., McHugh, P. J., Walsh, T. R., McDonough, M. A. & Schofield, C. J. (2016). *Antimicrob. Agents Chemother.* **60**, 142–150.
Christopeit, T., Carlsen, T. J., Helland, R. & Leiros, H. K. (2015). *J. Med. Chem.* **58**, 8671–8682.
Docquier, J.-D., Lamotte-Brasseur, J., Galleni, M., Amicosante, G., Frère, J.-M. & Rossolini, G. M. (2003). *J. Antimicrob. Chemother.* **51**, 257–266.
Drawz, S. M. & Bonomo, R. A. (2010). *Clin. Microbiol. Rev.* **23**, 160–201.
Emsley, P., Lohkamp, B., Scott, W. G. & Cowtan, K. (2010). *Acta Cryst.* D**66**, 486–501.
Evans, P. (2006). *Acta Cryst.* D**62**, 72–82.
Evans, P. R. (2011). *Acta Cryst.* D**67**, 282–292.
Evans, P. R. & Murshudov, G. N. (2013). *Acta Cryst.* D**69**, 1204–1214.
Fast, W. & Sutton, L. D. (2013). *Biochim. Biophys. Acta*, **1834**, 1648–1659.
Garau, G., García-Sáez, I., Bebrone, C., Anne, C., Mercuri, P., Galleni, M., Frère, J.-M. & Dideberg, O. (2004). *Antimicrob. Agents Chemother.* **48**, 2347–2349.
Garcia-Saez, I., Docquier, J.-D., Rossolini, G. M. & Dideberg, O. (2008). *J. Mol. Biol.* **375**, 604–611.
Gasteiger, E., Hoogland, C., Gattiker, A., Duvaud, S., Wilkins, M. R., Appel, R. D. & Bairoch, A. (2005). *The Proteomics Protocols Handbook*, edited by J. M. Walker, pp. 571–607. Totowa: Humana Press.
Gelin, M., Delfosse, V., Allemand, F., Hoh, F., Sallaz-Damaz, Y., Pirocchi, M., Bourguet, W., Ferrer, J.-L., Labesse, G. & Guichou, J.-F. (2015). *Acta Cryst.* D**71**, 1777–1787.
Kabsch, W. (2010). *Acta Cryst.* D**66**, 125–132.
King, D. T., Worrall, L. J., Gruninger, R. & Strynadka, N. C. J. (2012). *J. Am. Chem. Soc.* **134**, 11362–11365.
Lucasti, C., Vasile, L., Sandesc, D., Venskutonis, D., McLeroth, P., Lala, M., Rizk, M. L., Brown, M. L., Losada, M. C., Pedley, A., Kartsonis, N. A. & Paschke, A. (2016). *Antimicrob Agents Chemother.* **60**, 6234–6243.
McCoy, A. J., Grosse-Kunstleve, R. W., Adams, P. D., Winn, M. D., Storoni, L. C. & Read, R. J. (2007). *J. Appl. Cryst.* **40**, 658–674.
Mueller, U., Darowski, N., Fuchs, M. R., Förster, R., Hellmig, M., Paithankar, K. S., Pühringer, S., Steffien, M., Zocher, G. & Weiss, M. S. (2012). *J. Synchrotron Rad.* **19**, 442–449.
Poirel, L., Naas, T., Nicolas, D., Collet, L., Bellais, S., Cavallo, J. D. & Nordmann, P. (2000). *Antimicrob. Agents Chemother.* **44**, 891–897.
Wallace, A. C., Laskowski, R. A. & Thornton, J. M. (1995). *Protein Eng.* **8**, 127–134.
World Health Organization (2014). *Antimicrobial Resistance: Global Report on Surveillance*. Geneva: World Health Organization. http://www.who.int/drugresistance/documents/surveillancereport/en/.
Yamaguchi, Y., Jin, W., Matsunaga, K., Ikemizu, S., Yamagata, Y., Wachino, J., Shibata, N., Arakawa, Y. & Kurosaki, H. (2007). *J. Med. Chem.* **50**, 6647–6653.
Yang, S.-K., Kang, J. S., Oelschlaeger, P. & Yang, K.-W. (2015). *ACS Med. Chem. Lett.* **6**, 455–460.
Zhai, L., Zhang, Y.-L., Kang, J. S., Oelschlaeger, P., Xiao, L., Nie, S.-S. & Yang, K.-W. (2016). *ACS Med. Chem. Lett.* **7**, 413–417.
Zhang, Y.-L., Yang, K.-W., Zhou, Y.-J., LaCuran, A. E., Oelschlaeger, P. & Crowder, M. W. (2014). *ChemMedChem*, **9**, 2445–2448.